Hindawi
Mathematical Problems in Engineering
Volume 2021, Article ID 8324926, 11 pages
https://doi.org/10.1155/2021/8324926

Research Article

Control Strategy of Microgrid Inverter Based on H_∞ State Feedback Repeated Deadbeat Control

Ren Xie, Yougui Guo, and Yonghong Lan

College of Automation and Electronic Information, Xiangtan University, Xiangtan Hunan, China

Correspondence should be addressed to Yougui Guo; 719983182@qq.com

Received 19 September 2021; Accepted 18 November 2021; Published 21 December 2021

Academic Editor: Guoqiang Wang

Aiming at the voltage distortion at the microgrid public connection point caused by nonlinear loads, a H_∞ state feedback deadbeat repetitive control strategy is proposed to rectify the total harmonic distortion of the output voltage. Firstly, through establishing the state space of the repetitive controller, introducing state feedback, combining the H_∞ control theory, and reformulating the system stability problem as a convex optimization problem with a set of linear matrix inequality (LMI) constraints to be solved, high stability control accuracy can be guaranteed and antiharmonic interference strengthened. Secondly, by introducing deadbeat control technology to improve the transient response speed of the system, changes in output voltage caused by load changes can be quickly compensated. Compared with the existing methods, the designed control method has the advantages of good stability, low harmonic content, and fast convergence speed, and the results are easier to verify. Finally, the simulation verifies the effectiveness of the proposed control strategy.

1. Introduction

In recent years, the microgrid has received wide attention for its unique form of maximizing the flexibility and advantages of distributed generation systems (DG) [1–3]. Its internal energy conversion is mainly conducted via power electronics, and the inverter is the core link of the distributed generation system, its operating state is related to the performance of the whole system, and z-source inverter is widely used because of its function of voltage-up and step-down conversion. When the microgrid runs in the island mode, affected by the harmonic current generated by the nonlinear loads, the voltage at the Point of Common Coupling is thus distorted, leading to the degradation of the supply voltage quality and affecting the normal operation of the load and inverter [4–6]. Therefore, it is of great practical significance to study a control strategy for reducing the total harmonic distortion (THD) of the output voltage in a state of satisfying the demand for nonlinear loads.

Proportional integral (PI) control, though deficient [7, 8] for harmonic suppression, is widely used in microgrid inverters due to its easily realized structure, and the repetitive control, taking the advantage of its convenient implementation, easily realized structure, and high efficient waveform control, is widely applied to control the inverters, but the response speed is slow [9]. To enhance the robustness of the system, [10] proposes a combined controller for repetitive and sliding mode control and adds feedforward control to improve its dynamic properties, but the design of phase advance units and low-pass filters is complex. Document [11] proposed a method based on mixed sensitivity to determine repetitive control parameters. However, it takes efforts to choose weight function. Document [12, 13] proposed a design method of H_∞ control theory to obtain a stable compensator to improve its robustness, but compensators with good performance are often high-end and complex to implement. Most of the repetitive control design techniques mentioned in the literature are based on the transfer function method, which is not sufficient to deal with the time-varying uncertainty caused by the load change. Not only is the solution process complicated, but also the steady-state error and phase angle margin are used to judge the system performance after consulting the benchmark amount, which is often determined through heuristics.

Deadbeat control is widely studied in terms of its fast response speed and easy implementation, rather than its

poor robustness [13]. Document [14] proposes an improved deadbeat control strategy to compensate for the delay caused by the digital implementation by predicting the system behavior, but it needs to select large orders to ensure the accuracy of the algorithm prediction, which makes the calculation process complicated.

Inspired by the above literature, in order to reduce the harmonic content of the PCC point voltage of the z-source inverter with nonlinear loads and achieve power sharing, this paper proposes a H_∞ state feedback deadbeat repetitive control based on a parameter-optimized droop controller (H_∞SFDBRC) strategy. Aiming at the disadvantages of traditional repetitive control being insufficient to deal with the time-varying uncertainty caused by load changes, the complexity of the solution process, and the difficulty of verifying conditions, this paper designs an improved repetitive control system that optimizes the design of the repetitive controller, constructs a state space expression formula, and introduces H_∞ state feedback control, and thus the design of the repetitive controller is transformed into a convex optimization problem with a set of LMI constraints according to the Lyapunov functional; due to the inherent delay characteristics of repetitive control, in order to improve the transient performance of the system to obtain better antidisturbance characteristics, a new conceptual topology is proposed, with the deadbeat control technology, to provide fast dynamic response after the start of the system or during the large load step changes. A simulation model was built on the MATLAB/Simulink simulation platform, and the simulation results verified the effectiveness of the control strategy.

2. System Structure

The single-phase off-grid inverter system based on z-source inverter is shown in Figure 1. The designed control system has three constituent modules: repeated control, deadbeat control, and droop control modules. L_f and C_f are the filter inductors and capacitors, R_{Lf} is an equivalent series resistance of the filter inductance, R_i and L_i are the line impedance, I_{Labc} is an inductor current, u_C is the capacitor voltage, V_{0abc} is the output voltage, K_{11}, K_{12}, and K_2 are competitive controller coefficients calculated by LMI, $Q(s)$ $e^{-s\tau}$ is a first-order low-pass filter, K_3, K_4, K_5, and K_6 are the coefficients of the deadbeat control system, u_k is the SVPWM voltage modulation signal, k_p and k_q are droop coefficients, f_0 is the rated frequency, U_0 is the voltage amplitude when output reactive power is zero, and P, Q are measured values of active and reactive power, respectively. The measured inverter output voltage V_{0abc} and filter inductor current I_{Labc} are converted, by Park Formation, into voltage V_{0abc} and current I_{Labc} on the two-phase rotating coordinates. The input of voltage V_{0dq} and current I_{Labc} into the droop control system generates reference voltage r, which is then converted into modulate wave signals under the repetitive and deadbeat control. After controlling the inverter's on-off switch pipe, the effective tracking of the voltage signal can be realized.

Figure 1 shows the simplified topology of the droop control outer loop and the voltage control inner loop (Figure 2).

The z-source inverter consists of two capacitors and two inductors to form an X-type network, which connects the DC source with the three-phase inverter. The function of the diode is to prevent the current from flowing back to the DC side. In normal operation, there are two states of straight-through and nonstraight-through; when the upper and lower power devices of the same bridge arm are turned on at the same time, it is in the straight-through state, through which the z-source inverter can flexibly boost and step down; the nonstraight-through state refers to the traditional inverter state. Figures 3 and 4 are equivalent circuits in both straight-through and nonstraight-through states, respectively.

Since the three-phase filter circuit parameters are consistent and the d_q-axis is independent after the coordinates are transformed, simply analyze the d-axis single-phase LC filter as shown in Figure 5; the DC voltage, z-source network, and inverter are equivalent to a voltage source $u(t)$, where the influence of both the linear and nonlinear loads on the controlled output voltage is modeled by the uncertain load admittance $Y_0(t)$ and the external current source $i_d(t)$.

Select inductor current I_{Ld} and capacitor voltage V_{0d} as state variables to establish circuit equations according to Kirchhoff's law

$$\begin{cases} u(t) = L_f \dfrac{\mathrm{d}I_{Ld}(t)}{\mathrm{d}t} + R_{Lf} I_{Ld}(t) + V_{0d}(t), \\ I_{Ld}(t) = C_f \dfrac{\mathrm{d}V_{0\,d}(t)}{\mathrm{d}t} + V_{0d}(t) Y_0(t) + i_d(t). \end{cases} \tag{1}$$

Organize it into a matrix form

$$\begin{bmatrix} \dfrac{\mathrm{d}I_{Ld}(t)}{\mathrm{d}t} \\ \dfrac{\mathrm{d}V_{0d}(t)}{\mathrm{d}t} \end{bmatrix} = \begin{bmatrix} -\dfrac{R_{Lf}}{L_f} & -\dfrac{1}{L_f} \\ \dfrac{1}{C_f} & \dfrac{Y_0(t)}{C_f} \end{bmatrix} + \begin{bmatrix} \dfrac{1}{L_f} \\ 0 \end{bmatrix} u(t) + \begin{bmatrix} 0 \\ \dfrac{1}{C_f} \end{bmatrix} i_d(t),$$

$$V_{0d}(t) = \begin{bmatrix} 0 & 1 \end{bmatrix} \begin{bmatrix} I_{Ld}(t) \\ V_{0d}(t) \end{bmatrix}. \tag{2}$$

If $x(t) = [I_{Ld}(t)\ V_{0d}(t)]^T$, it can be written as a state space expression.

$$\begin{cases} \dot{x}(t) = \mathbf{A}(Y_0(t))\mathbf{x}(t) + \mathbf{B}u(t) + \mathbf{B}_d i_d(t), \\ y(t) = \mathbf{C}\mathbf{x}(t), \end{cases} \tag{3}$$

where $x(t) \in R$ is the state vector of the inverter, $u(t) \in R$ is control input, $y(t) \in R$ is control output, $i_d(t) \in R$ is periodic interference, and $A(Y_0(t))$ is the matrix function of the uncertain parameter $Y_0(t)$.

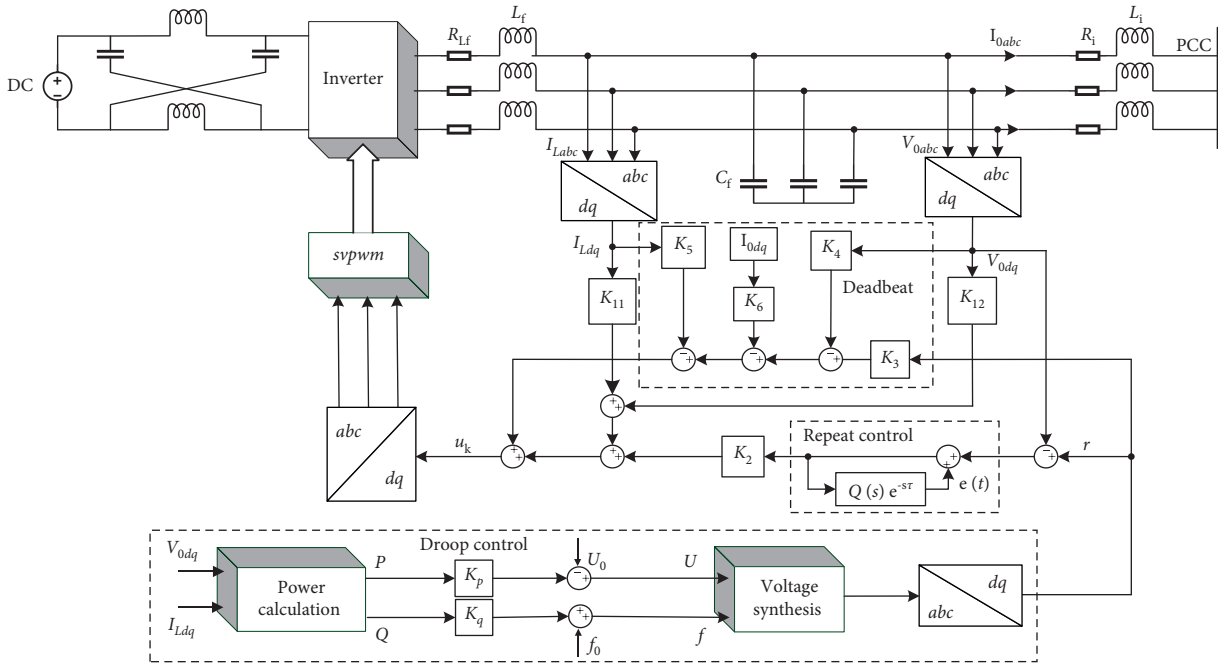

Figure 1: Control block diagram of island microgrid inverter.

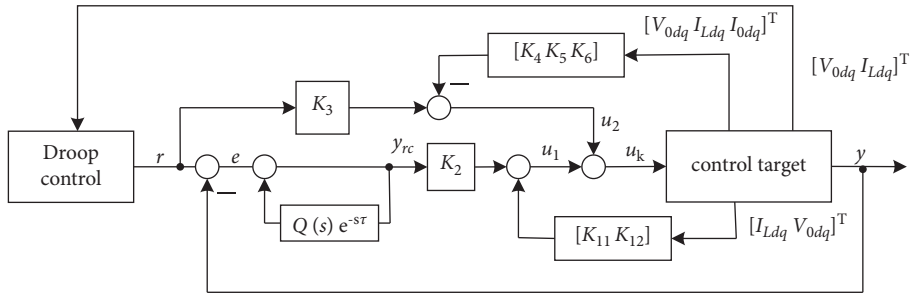

Figure 2: System simplified control topology diagram.

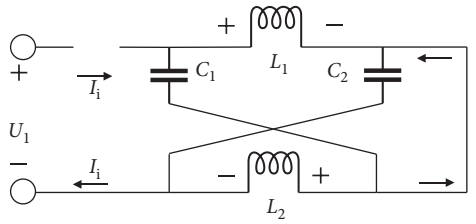

Figure 3: Straight-through commutation state.

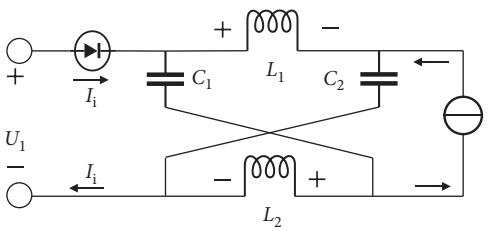

Figure 4: Nonstraight-through commutation state.

Suppose that the minimum and maximum values of the $Y_0(t)$ are known

$$Y_{\min} \le Y_0(t) \le Y_{\max}. \tag{4}$$

The parameter $Y_0(t)$ is usually converted according to its nominal value Y_N and the deviation Y_D, as follows:

$$Y_0(t) = Y_N + \delta(t) Y_d, \quad \delta(t) \in [-1, 1], \tag{5}$$

where $Y_N = Y_{\min} + Y_{\max}/2, Y_d = Y_{\min} - Y_{\max}/2$.

According to (5)

$$\mathbf{A}(Y_0(t)) = \mathbf{A}(Y_N) + \mathbf{H}(Y_d)\delta(t)\mathbf{E}, \quad \delta(t) \in [-1, 1], \tag{6}$$

where $A(Y_N)$, $H(Y_D)$, and E are the constant matrix of the uncertain structures, as given by the following formula:

$$\begin{aligned} \mathbf{A}(Y_N) &= \begin{bmatrix} -\dfrac{R_{Lf}}{L_f} & -\dfrac{1}{L_f} \\ \dfrac{1}{C_f} & -\dfrac{Y_N}{C_f} \end{bmatrix}, \\ \mathbf{H}(Y_d) &= \begin{bmatrix} 0 & 0 \\ 0 & -\dfrac{Y_d}{C_f} \end{bmatrix}, \\ \mathbf{E} &= I_2. \end{aligned} \tag{7}$$

2.1. Voltage Control Strategy. Repetitive control is to reflect the deviation from the previous operation to the present and add it to the controlled object together with the "current deviation" for control to improve tracking accuracy and suppress periodic interference. However, such closed-loop systems have infinite poles on the virtual axis. It is impossible to achieve stability through classical control methods.

Figure 6 shows a repetitive controller with a low-pass filter; set the low-pass filter $Q(s)$ as

$$\begin{aligned} Q(s) &= \frac{\omega_c}{s + \omega_c}, \\ \omega_c &= \frac{1}{T}, \end{aligned} \tag{8}$$

where ω_c and T are the corner frequency and time constants of the first-order low-pass filters, respectively. The method of determining the size of ω_c is as follows:

$$\begin{cases} |q(j\omega)| \approx 1, & \omega \ll \omega_0, \\ |q(j\omega)| < 1, & \omega > \omega_0, \end{cases} \tag{9}$$

where ω_0 is the frequency bandwidth of the modulation reference signal: $\omega_0 = 2\pi/\tau$.

From Figure 6, the transfer function of the repeated controller is

$$G_{rc}(s) = \frac{1}{1 - Q(s)e^{-s\tau}}. \tag{10}$$

Deduced from formulas (8) and (9), the state space of formula (9) is available

$$\begin{cases} \dot{x}_{rc}(t) = -\omega_c x_{rc}(t) + \omega_c x_{rc}(t - \tau) + \omega_c e(t - \tau), \\ y_{rc}(t) = x_{rc}(t) + e(t), \end{cases} \tag{11}$$

where $x_{rc}(t)$ is a low-pass filter state variable.

2.2. Design of H_∞ State Feedback Repetitive Controller. Construct the augmentation vector as follows:

$$\mathbf{Z}(t) = \begin{bmatrix} \mathbf{x}(t) \\ x_{rc}(t) \end{bmatrix} \in R^{(n+1)}. \tag{12}$$

Rules (3) and (11) can be converted to

$$\dot{Z}(t) = (\mathbf{A}_a + \Delta\mathbf{A}_a(t))\mathbf{Z}(t) + \mathbf{A}_d\mathbf{Z}(t - \tau) + \mathbf{B}_a u(t) + \mathbf{B}_q\mathbf{q}(t), \tag{13}$$

where

$$\begin{aligned} \mathbf{q}(t) &= [\, r(t) \;\; i_d(t) \,]' \in R^2, \\ \mathbf{A}_a &= \begin{bmatrix} \mathbf{A}(Y_N) & 0_{2\times1} \\ 0_{1\times2} & -\omega_c \end{bmatrix}, \\ \mathbf{B}_a &= \begin{bmatrix} \mathbf{B} \\ 0 \end{bmatrix}, \\ \mathbf{A}_d &= \begin{bmatrix} 0_{1\times2} & 0 \\ -\mathbf{C}\omega_c & \omega_c \end{bmatrix}, \\ \Delta\mathbf{A}_a(t) &= \mathbf{H}_a\delta(t)\mathbf{E}_a \\ \mathbf{H}_a &= \begin{bmatrix} \mathbf{H}(Y_d) \\ 0_{1\times2} \end{bmatrix}, \\ \mathbf{E}_a &= \begin{bmatrix} E' \\ 0'_{1\times2} \end{bmatrix}', \\ \mathbf{B}_q &= \begin{bmatrix} 0_{2\times1} & \mathbf{B}_d \\ \omega_c & 0 \end{bmatrix}. \end{aligned} \tag{14}$$

As shown from Figure 7, the control rate in the closed-loop system (13) is

$$u_1(t) = \mathbf{K}_1 x(t) + K_2 y_{rc}(t), \tag{15}$$

where $\mathbf{K}_1 = [\, K_{11} \;\; K_{12} \,]$.

Override the $u_1(t)$

$$u_1(t) = \mathbf{F}\mathbf{Z}(t) + K_2 r(t), \tag{16}$$

where $\mathbf{F} \in R^{1\times(n+1)} = [(\mathbf{K}_1 - K_2\mathbf{C})\, K_2]$.

Then the augmented system (13) is rewritten as

$$\dot{Z}(t) = (\mathbf{A}_\Delta + \mathbf{B}_a\mathbf{F})\mathbf{Z}(t) + \mathbf{A}_0\mathbf{Z}(t - \tau) + \overline{\mathbf{B}}_q\mathbf{q}(t), \tag{17}$$

where $A_\Delta = \mathbf{A}_a + \Delta\mathbf{A}_a(t)$, and $\overline{\mathbf{B}}_q$ depends on K_2

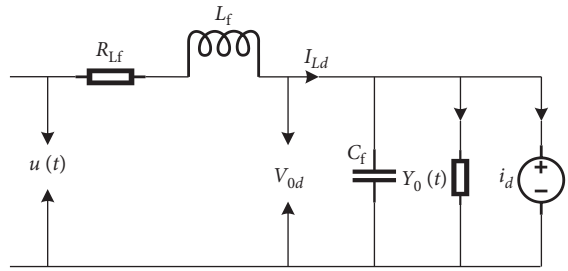

Figure 5: LC filter single-phase equivalent circuit.

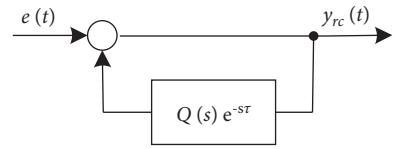

Figure 6: Low-pass filter repetitive control topology.

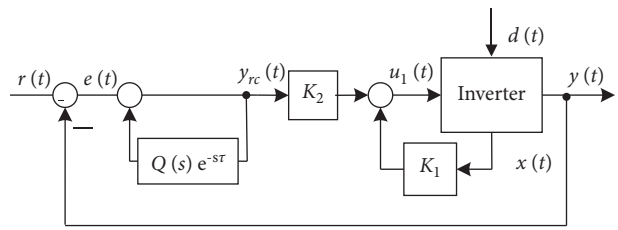

Figure 7: Repetitive control topology.

$$\overline{\mathbf{B}}_q = \begin{bmatrix} \mathbf{B}K_2 & \mathbf{B}_d \\ \omega_c & 0 \end{bmatrix}. \tag{18}$$

To validate the stability of the above system, ignoring the external input $q(t)$, the closed-loop system can be abbreviated as

$$\dot{Z}(t) = (\mathbf{A}_\Delta + \mathbf{B}_a\mathbf{F})\mathbf{Z}(t) + \mathbf{A}_d\mathbf{Z}(t-\tau). \tag{19}$$

Then for a given cutoff frequency ω_c, the gain F needs to be determined so that the system is asymptotically stable for any $Y_0(t)$.

In view of the above augmented system, performance criteria are introduced:

$$J(p(t)) \coloneqq \|p(t)\|_2^2 = \int_0^\infty p(t)'p(t)\mathrm{d}t, \tag{20}$$

where $p(t)$ defines the performance output for

$$p(t) \coloneqq \mathbf{C}_p z(t) + \mathbf{D}_p u(t), \tag{21}$$

where C_p and D_p are the constant matrix of the appropriate dimensions.

Further ensure that the system trajectory has a given exponential decay rate of α

$$\|\mathbf{Z}(t)\| \le \beta\|\mathbf{Z}(0)\|e^{-\alpha t}, \quad t > 0, \tag{22}$$

where β is a positive scalar and $Z(0)$ is the initial state.

$$\mathbf{Z}(\phi) = 0, \quad \forall\phi \in [-\tau, 0). \tag{23}$$

In order to obtain a sufficient condition for the robust asymptotic stability of system (19), according to [16], the above problem can be solved by the following lemma.

Lemma 1 (see [15]). *For the given positive scalars ω_c and α, consider formulas (17) and (21). Suppose there is a symmetric positive definite matrix W, $S \in R^{3\times3}$, matrix $Y \in R^{1\times3}$, and positive scalars λ and ν are satisfied with*

$$\begin{bmatrix} \Gamma(\mathbf{W},\mathbf{S},\upsilon) & e^{\alpha t}\mathbf{A}_d\mathbf{W} & \mathbf{W}\mathbf{E}_a & \mathbf{W}\mathbf{C}_p' + Y'\mathrm{D}_p' \\ e^{\alpha t}\mathbf{W}A'_{\mathrm{d}} & -\mathbf{S} & 0_{3\times3} & 0_{3\times1} \\ E_a'\mathbf{W} & 0_{3\times3} & -\upsilon\mathbf{I}_3 & 0_{3\times1} \\ \mathbf{C}_p\mathbf{W} + \mathbf{D}_p\mathbf{Y} & 0_{1\times3} & 0_{1\times3} & -\lambda \end{bmatrix} < 0, \tag{24}$$

where $\Gamma(\mathbf{W},\mathbf{S},\upsilon) = \mathbf{A}_a\mathbf{W} + \mathbf{W}\mathbf{A}_a' + 2\alpha\mathbf{W} + \mathbf{B}_a\mathbf{Y} + Y'\mathbf{B}_a' + \mathbf{S} + \upsilon\mathbf{H}_a\mathbf{H}_a'$.

Then the closed-loop system in equation (17) is gradually stable when the gain $\mathbf{F} = \mathbf{Y}\mathbf{W}^{-1} = [\,\mathbf{F}_1 \;\; \mathbf{F}_2\,]$.

Note 1. Lemma 1 gives the stability conditions of H_∞ repetitive control when the inverter carries an uncertain load and the design method of the state feedback control rate. It shows that the closed-loop system (19) is progressively stable, so the closed-loop system (17) is internally stable.

In this paper, LMI is used to optimize the design of the repetitive controller, and the MATLAB toolbox is used to solve it. Compared with the traditional repetitive controller design method that determines, by heuristics, reference quantity, like steady-state error and phase angle margin, this paper acquires them by solving the linear matrix inequality and at the meantime simplifies the design process by reducing the number of filters and the cost of the whole system, facilitating the solution of the time-varying uncertainty caused by load change. See Table 1 for the inverter parameters involved.

Take $\omega_c = 1000$ and $\alpha = 155$, and the parameters of the repetitive controller obtained by using LMI according to Lemma 1 are

$$\begin{aligned} \mathbf{K}_1 &= \left[-181.2753 \quad -153.7798 \right], \\ K_2 &= 5.2749 \times 10^3, \end{aligned} \tag{25}$$

2.3. H_∞ State Feedback Deadbeat Repetitive Control. Due to the inherent nature of the delay characteristic of the repetitive controller, the dynamic performance of the system is poor. While deadbeat control has the advantages of quick instantaneous reaction and low harmonic distortion rate, in order to improve the dynamic performance of the system, compensate for the distortion caused by the dead time of the switch, introduce deadbeat control technology, and propose a new conceptual topology as shown in Figure 8.

The sampling principle of deadbeat control is shown in Figure 9, the sampling period is expressed as T, the output value of the inverter is expressed as $+E$ and $-E$, $\Delta T(K)$ represents the adjusting width of the K th cycle square wave, and the same $\Delta T(K)$ represents the width of the $K+1$ th cycle. The voltage value in the sampling period is determined by the sampling value at that time and the reference value at the next time.

When the microgrid inverter is working, the introduced deadbeat control technology takes into account the effect of the actual load current, so that the entire system can automatically compensate for load disturbances during the transient performance, so that it can be used during system startup or load step. It provides fast dynamic response during the change period.

The system adopts discrete-time simulation. The reason why the digital system can achieve the deadbeat control effect is that the output of the next beat of the system can always be expressed as a linear combination of the current input control quantity and the system state variable. When the system deviates from the reference value, it will respond quickly. The load disturbance is compensated and the pulse width of the next switching period is calculated. According to the state space expression of formula (3), it is to discretize on the equivalent impulse principle; since the deadbeat controller is mainly used to provide rapid dynamic response during system startup or load step responses, to simplify the calculation, taking $Y_0(t)$ as a fixed value is available to

$$\begin{cases} x(k+1) = \mathbf{G}x(k) + \mathbf{M}_1 u_2(k) + \mathbf{M}_2 I_{0d}(k), \\ y(k) = \mathbf{C}x(k), \end{cases} \tag{26}$$

where I_{0d} is the d-axis load current.

$$\begin{aligned} \mathbf{G} &= e^{\mathbf{A}(Y_0)T_s} = \begin{bmatrix} g_{11} & g_{12} \\ g_{21} & g_{22} \end{bmatrix}, \\ \mathbf{x}(k) &= \begin{bmatrix} V_{0d}(k) \\ I_{Ld}(k) \end{bmatrix}, \\ \mathbf{M}_1 &= \mathbf{A}(Y_0)^{-1}\left(e^{\mathbf{A}(Y_0)T_s} - \mathbf{I}\right)\mathbf{B} = \left[m_{11} \quad m_{12} \right]^T, \\ \mathbf{M}_2 &= \mathbf{A}(Y_0)^{-1}\left(e^{\mathbf{A}(Y_0)T_s} - \mathbf{I}\right)\mathbf{B}_d = \left[m_{21} \quad m_{22} \right]^T. \end{aligned} \tag{27}$$

Expanded by formula (26)

$$\begin{cases} V_{0d}(k+1) = g_{11}V_{0d}(k) + g_{12}I_{Ld}(k) + m_{11}u_2(k) + m_{21}I_{0d}(k), \\ I_{Ld}(k+1) = g_{21}V_{0d}(k) + g_{22}I_{Ld}(k) + m_{12}u_2(k) + m_{22}I_{0d}(k). \end{cases} \tag{28}$$

According to formula (28), the capacitor voltage $V_{0d}(k+1)$ at t_{k+1} time is determined by $V_{0d}(k)$, $I_{Ld}(k)$, and $u_2(k)$ at t time. Conversely, if $V_{0d}(k+1)$, $V_{0d}(k)$, and $I_{Ld}(k)$ are known at t_k time, then the output voltage $u_2(k)$ at t_k time can be calculated. The calculation formula can be derived from formula (28):

$$u_2(k) = \frac{1}{m_{11}}\left[V_{0d}(k+1) - g_{11}V_{0d}(k) - g_{12}I_{Ld}(k) - m_{21}I_{0d}(k)\right]. \tag{29}$$

In fact, both $V_{0d}(k)$ and $I_{Ld}(k)$ are t_k time sampling values, which are known. Now let us determine the capacitor voltage $V_{0d}(k+1)$ at the time of t_{k+1}. It can be seen from formula (28) that the output of the system is the capacitor voltage and the ideal output voltage of the inverter is the standard sinusoidal reference voltage. Therefore, the reference voltage $r(k+1)$ of t_{k+1} can be used instead of the capacitor voltage $V_{0d}(k+1)$ of t_{k+1}, that is,

$$\begin{aligned} u_2(k) &= \frac{1}{m_{11}}\left[r(k+1) - g_{11}V_{0d}(k) - g_{12}I_{Ld}(k) - m_{21}I_{0d}(k)\right] \\ &= K_3 r(k+1) - K_4 V_{0d}(k) - K_5 I_{Ld}(k) - K_6 I_{0d}(k). \end{aligned} \tag{30}$$

System integrated control law $u_k = u_1 + u_2$; therefore, it is necessary to obtain the discrete-time model of u_1, where $K_1 x(t)$ is obtained from static feedback and does not require a discretization process. $K_2 y_{rc}(t)$ is derived from the dynamic compensator and must be discretized to determine the relationship between $y_{rc}(t)$ and $e(t)$. Discretization of equation (10) can obtain the discrete-time transfer function from $e(z)$ to $y_{rc}(z)$

$$G_{rc}(z) = \frac{(2+\omega_t) + (\omega_t - 2)z^{-1}}{(2+\omega_t) + (\omega_t - 2)z^{-1} - \omega_t z^{-\gamma} - \omega_t z^{-\gamma-1}}, \tag{31}$$

where $\omega_t = \omega_c T_s$, in terms of difference equations

Table 1: Inverter parameters.

Parameter	Value
Filter inductance L_f/mH	0.6
Filter capacitor C_f/μF	1500
Damping resistance R_L/Ω	0.01
Minimum admittance/S	0.0001
Maximum admittance/S	0.2
Switching frequency f/KHz	21.6
DC bus voltage/V	800

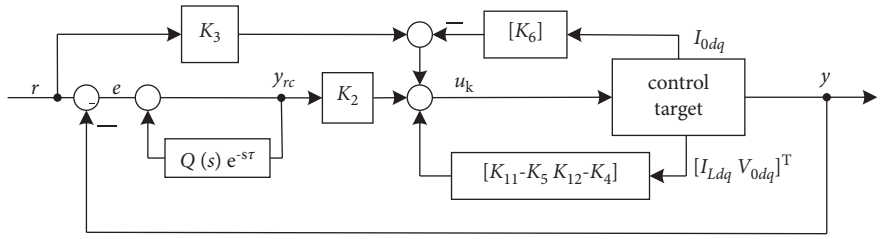

Figure 8: H_∞ state feedback repeated deadbeat control topology.

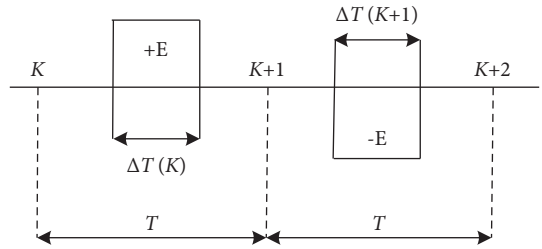

Figure 9: Structure diagram of deadbeat control sampling.

$$y_{rc}(k) = e(k) + \frac{-2+\omega_t}{2+\omega_t}\left[e(k-1) - y_{rc}(k-1)\right] + \frac{\omega_t}{2+\omega_t}\left[y_{rc}(k-\gamma) + y_{rc}(k-\gamma-1)\right]. \tag{32}$$

From equations (31) and (32),

$$u_1(k) = K_{11}I_{Ldq}(k) + K_{12}V_{0dq}(k) + K_2 y_{rc}(k). \tag{33}$$

The system control law is

$$u_k(k) = (K_{11}-K_5)I_{Ldq}(k) + (K_{12}-K_4)V_{0dq}(k) + K_2 y_{rc}(k) + K_3 r(k+1) - K_6 I_{0dq}(k). \tag{34}$$

According to the conclusion of the document [17], when the H_∞ state feedback repetitive control and deadbeat control act independently, the system is stable, so the composite system is also stable.

In summary, the design steps of the control law in this paper are as follows.

Step 1. Give suitable ω_c and α.

Step 2. Solve the following convex optimization problem:

$$\min_{W,Y,S,v,\lambda} \lambda \text{ Satisfaction.} \tag{35}$$

Step 3. Compute

$$\mathbf{F} = \mathbf{YW}^{-1} = [\,\mathbf{F}_1\ \ \mathbf{F}_2\,], \quad K_1 = F_1 + K_2 C, \quad K_2 = F_2. \tag{36}$$

Step 4. Solve the output voltage u_2 at $t = k$, and obtain the state feedback coefficient.

2.4. Droop Control. This paper studies the island mode of the inverter; the calculation formula of average active power P and average reactive power Q is as follows:

$$\begin{cases} P = \left(V_{0d}I_{Ld} + V_{0q}I_{Lq}\right)\dfrac{w_{f1}}{S+w_{f1}}, \\ Q = \left(V_{0d}I_{Lq} - V_{0q}I_{Ld}\right)\dfrac{w_{f2}}{S+w_{f2}}. \end{cases} \tag{37}$$

In the formula, w_{f1} and w_{f2} are the cutoff frequency of the low-pass filter.

The droop control equation is

$$\begin{cases} f = f_0 + k_q Q, \\ U = U_0 - k_p P. \end{cases} \tag{38}$$

In the formula, k_q and k_p are droop characteristic coefficients, f_0 is rated frequency, and U_0 is voltage amplitude when output reactive power is 0. The control parameters are shown in Table 2.

2.5. Simulation Verification. This paper establishes a microgrid operation simulation model with two DG on the MATLAB/Simulink software platform as shown in Figure 10. The DC bus voltage of DG module is maintained by ideal power source, which adopts the same LC filter and line impedance. The standard feeder impedance of low-voltage microgrid is $0.642 + j0.0083\ \Omega$/km. The line impedance seen from DG1 and DG2 is $1.284 + j0.0166\ \Omega$/km. The common load load3 is connected to the common AC bus of the microgrid and through on and off switch K.

In order to verify the effectiveness of the control strategy proposed in this paper, the following simulation experiments are carried out. The load is a rectifier with a $21.8\ \Omega$ output in parallel with a set of $10.9\ \Omega$ resistors.

Figure 11(a) shows the phase A output voltage during system startup. It can be seen that, due to the deadbeat control technology, the voltage has achieved good tracking in a very short time. As shown in Figure 11(b), the periodic error signal begins to fluctuate and then quickly converges to a very small level (less than 0.5 V), and the entire system is stable. Then apply a large load step change test to check the system control performance. At the 0.4 s time point, the nonlinear load suddenly increases from one group to two groups. Figure 12(a) shows the corresponding PCC point voltage and current changes. It can be seen that, for large load step changes, the system is robust and withstands variation. Figure 12(b) shows the changes of active power and reactive power when the system load changes step by step. It can be seen that the system can still maintain a stable and equal distribution of active and reactive power when the load step changes, and the power fluctuates in it tending to be stable in a short period of time, indicating that the proposed control strategy has good anti-interference performance and dynamic response performance.

According to the comparison method of [18], the proposed H_∞ state feedback deadbeat repetitive control is compared with H_∞ repetitive control and PI control (hereinafter referred to as H_∞SFDBRC, H_∞RC, and PI), in which H_∞ repetitive control and PI control are designed by ourselves, and other conditions such as inverter parameters and line impedance are consistent. It is proved that the designed control strategy can improve the performance of inverter PCC point voltage THD under nonlinear load.

When using PI control, the PCC point voltage waveform, voltage error, and spectrum analysis results are shown in Figure 13(a). It can be seen from the figure that the PCC point voltage waveform has obvious distortion, the steady-state error is the largest, and the tracking performance is poor. The quality of the grid-connected voltage waveform is poor, and the voltage harmonic content is 4.91%.

Table 2: Droop control parameters.

Parameter	Value
Line impedance/Ω	$1.284 + j0.0166$
Filter parameters	$w_{f1} = 50$; $w_{f2} = 100$
Rated frequency/Hz	50
Voltage amplitude/V	110
Droop coefficient	$k_p = 10^{-5}$, $k_q = 3 \times 10^{-4}$

When using H_∞RC, the PCC point voltage waveform, voltage error, and spectrum analysis results are shown in Figure 13(b). The introduction to the internal model link enables the system to better compensate for the harmonic voltage, and the PCC point voltage waveform quality is better than PI control strategy, the voltage waveform is smoother, the harmonic compensation effect is good, the voltage harmonic content is 2.44%, and the steady-state error is better than PI control, but the dynamic response speed is slow.

When using H_∞SFDBRC, the PCC point voltage waveform, voltage error, and spectrum analysis results are shown in Figure 13(c). At this time, the system steady-state error is the smallest, and the excellent tracking performance significantly improves the voltage waveform quality. The deadbeat control technology with the introduction to the system enhances the anti-interference performance of the system, enabling the system to quickly respond to various sudden problems. The quality of the voltage waveform is better than the first two control strategies, and the harmonic compensation effect is very good, and the voltage harmonic content is only 0.67%.

In order to further verify the feasibility of the proposed scheme, the PCC point voltage waveform and power changes in the following two cases are simulated. Under the situation, only the inverter DG1 runs when the system starts, and the DG2 switch is closed at 0.4 s, and the simulation time is 1s. The simulated waveforms are shown in Figures 14(a)–14(c). When the microgrid is operating normally, it is connected to DG2 for interconnection at 0.4 s. DG1 and DG2 maintain a good coordinated operation. The PCC voltage quickly returns to a stable sinusoidal curve after slight fluctuations, during which active power and reactive power can also move quickly to achieve power sharing and maintain stability. It can also move quickly to achieve power sharing and maintain stability.

In case two, the two inverters run in parallel, the simulation time is 1 s, the switch K_n is disconnected at 0.4 s, and DG2 exits operation. From the simulation waveform diagrams 14(d)–14(f), it can be seen that when the microgrid is running in parallel, when one of the DGs quits operation due to a fault, the microgrid can react quickly and reach a new stable state, where the PCC voltage is almost invariant and remains as a sine curve, and the distribution and transformation of active power and reactive power in this process also maintain extremely high accuracy.

In summary, the control strategy proposed in this article can still ensure the stability and normal operation of the microgrid when the DG is connected or disconnected or the load changes.

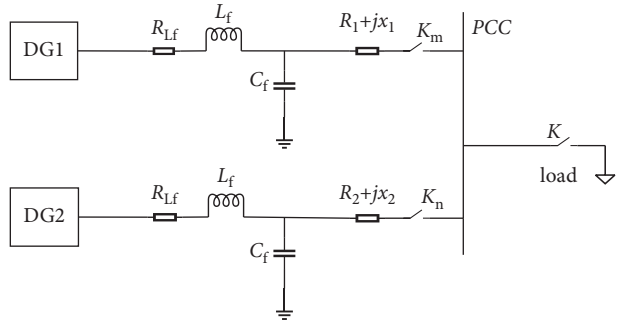

Figure 10: Microgrid simulation model.

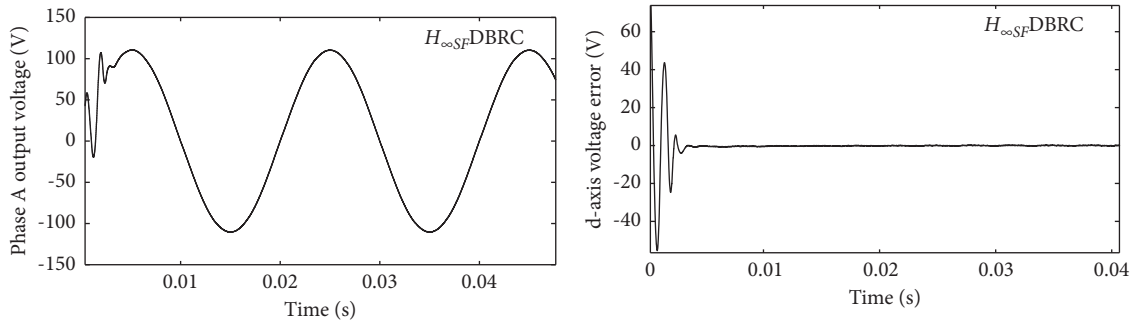

Figure 11: Output voltage of phase A during system startup and voltage error signal of d-axis seen by the repetitive controller. (a) Phase A output voltage. (b) d-axis voltage error obtained.

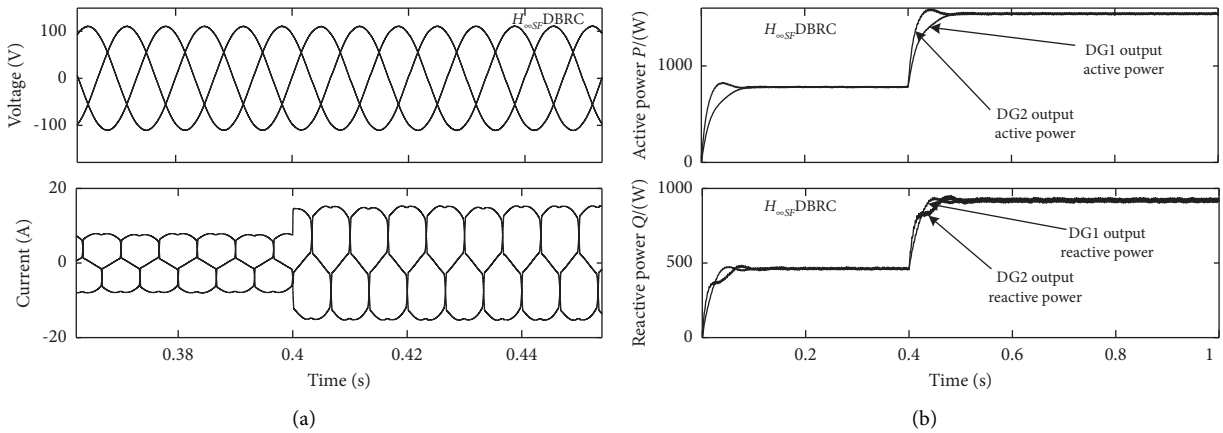

Figure 12: Three-phase output voltage during steady-state operation and three-phase voltage and current during load step changes. (a) PCC voltage and current. (b) Active and reactive power.

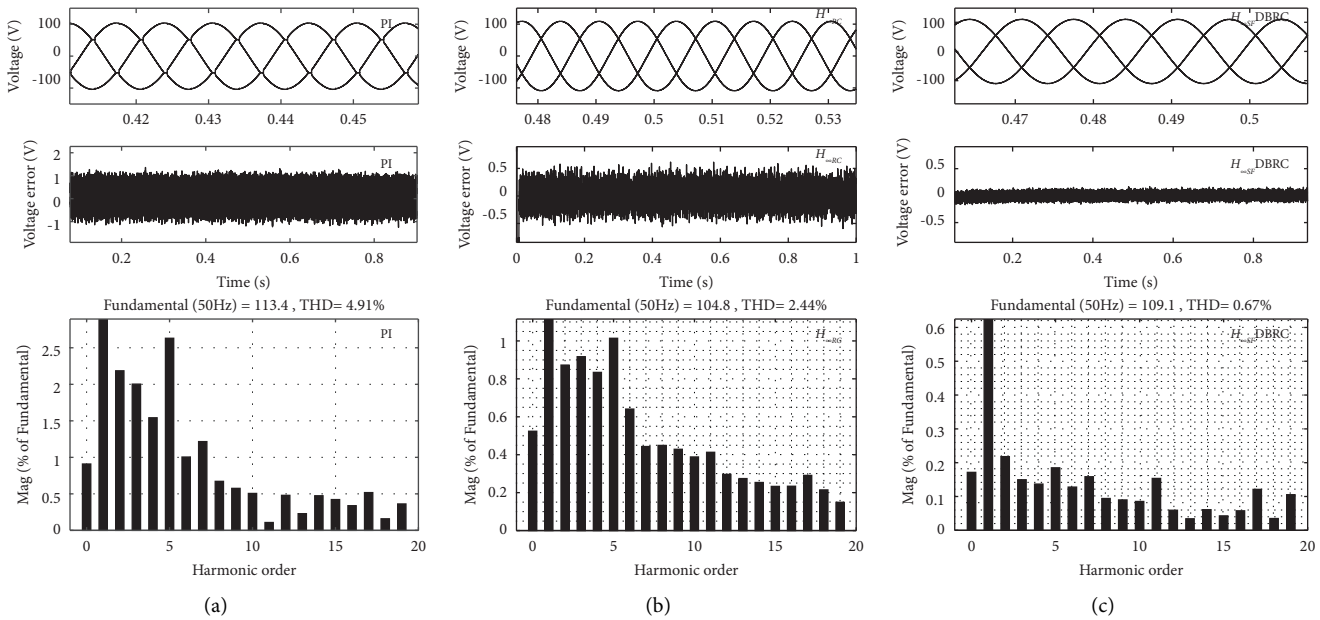

Figure 13: PCC point voltage, d-axis voltage error, and its THD value. (a) PI controller. (b) H_∞RC controller. (c) H_∞SFDBRC controller.

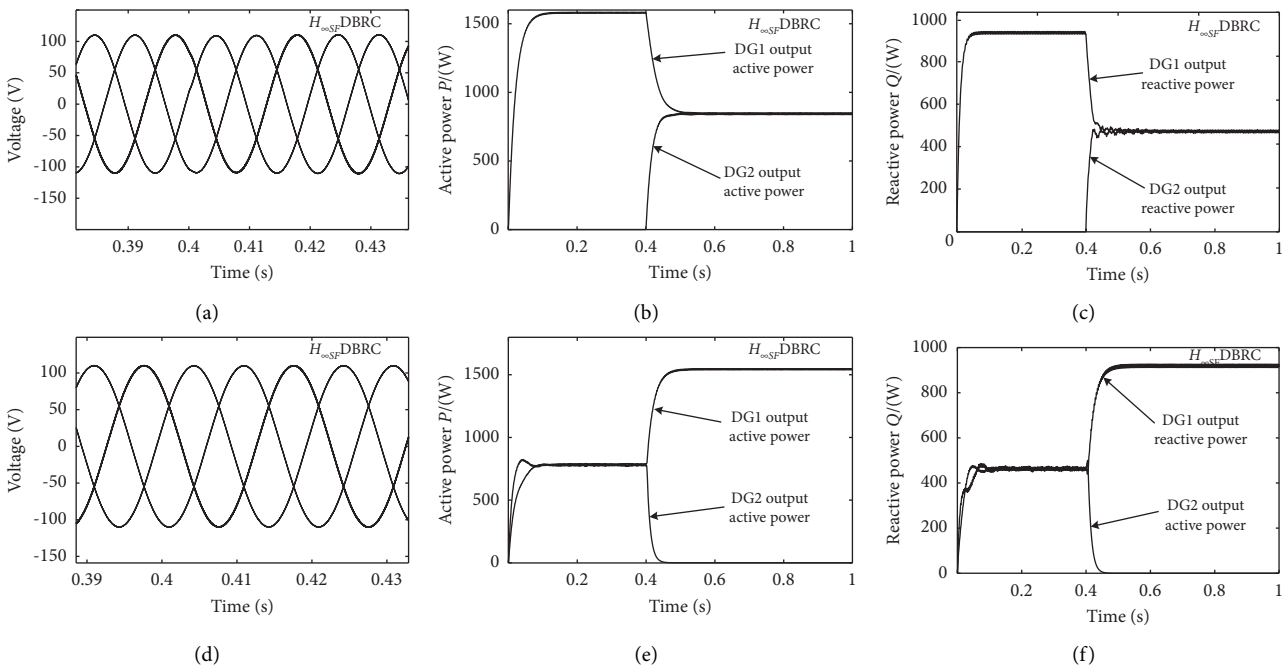

Figure 14: PCC voltage, DG output active, and reactive power. (a) PCC voltage waveform. (b) DG output active power. (c) DG output reactive power. (d) PCC voltage waveform. (e) DG output active power. (f) DG output reactive power.

3. Conclusion

Aiming at the problem of voltage distortion at the public grid connection point of island microgrid caused by nonlinear load, this paper designs a H_∞ state feedback deadbeat repetitive control strategy to reduce the total harmonic distortion of the output voltage. Through theoretical analysis and research, the following conclusions can be drawn.

(1) Lyapunov functional is used to optimize the design problem of repetitive controllers, the robustness of the closed-loop system is ensured by introducing state feedback, combined with H_∞ control theory, the design problem is transformed into a set of linear matrix inequality constraints' convex optimization problem, which can simplify the repetitive control design, and compared with the traditional design

method, the parameters representing the stability of the system can be accurately obtained and verified. It does not need to be obtained through repeated tests by trial method. It is more suitable for practical engineering applications and has the advantages of good stability, low harmonic content, and fast convergence speed.

(2) The introduction of deadbeat control technology not only effectively improves the response speed of the system, but also compensates for the distortion introduced by the switch dead time. Through simulation, we can find that the microgrid can quickly react and respond regardless of the actual system startup period or the large load step change period. A stable state is reached.

(3) The simulation results show that, compared with PI control and H_∞ repetitive control, the proposed control strategy can effectively reduce harmonics, improve the voltage quality at PCC point, and has good control performance under nonlinear load conditions.

Data Availability

The data used to support the findings of this study are included within the article. See Table 1 for the inverter parameters involved: parameters and values: z-source capacitor, C/μF, 4000, z-source inductor, L/mH, 0.5, filter inductor, Lf/mH, 0.6, filter capacitor, Cf/μF, 1500, damping resistance, RL/Ω 0.01, minimum admittance/S, 0.0001, maximum admittance/S, 0.2, switching frequency, f/KHz, 21.6, and DC bus voltage/V, 800. Take $\omega_c = 1000$ and $\alpha = 155$. The control parameters are shown in Table 2: parameters and value: line impedance/Ω $1.284 + j0.0166$, filter parameters $w_{f1} = 50$; $w_{f2} = 100$, rated frequency/Hz 50, voltage amplitude/V 110, and droop coefficient. $k_p = 10 - 5$ and $k_q = 3 \times 10 - 4$.

Conflicts of Interest

The authors declare that they have no conflicts of interest.

References

[1] M. A. Hossain, H. R. Pota, M. J. Hossain, and F. Blaabjerg, "Evolution of microgrids with converter-interfaced generations: challenges and opportunities," *International Journal of Electrical Power & Energy Systems*, vol. 109, no. JUL, pp. 160–186, 2019.

[2] D. Petreus, R. Etz, T. Patarau, and M. Cirstea, "An islanded microgrid energy management controller validated by using hardware-in-the-loop emulators," *International Journal of Electrical Power & Energy Systems*, vol. 106, no. MAR., pp. 346–357, 2019.

[3] P. Sreedharan, J. Farbes, E. Cutter, C. K. Woo, and J. Wang, "Microgrid and renewable generation integration: university of California, San Diego," *Applied Energy*, vol. 169, no. MAY1, pp. 709–720, 2016.

[4] C. Meng, X. X. Ning, and B. Z. Lai, "Hierarchical frequency control strategy of microgrids with virtual synchronous generators," *High Voltage Engineering*, vol. 44, no. 4, pp. 1278–1284, 2018.

[5] Z. Li, Z. Jiang, J. Huang, W. Ma, and Z. Huang, "Time-frequency voltage control strategy of microgrid inverter based on linear active disturbance rejection control," *Automation of Electric Power Systems*, vol. 44, no. 10, pp. 145–154, 2020.

[6] D. Li, B. Wang, J. Liu, and W. Xu, "Research on droop control method with the compounding feed forward compensation for micro-grid inverter," *Power Electronics*, vol. 54, no. 6, pp. 86–89+94, 2020.

[7] C. Bao, X. Ruan, X. Wang, D. Pan, W. Li, and K Weng, "Design of grid-connected inverters with LCL filter based on PI regulator and capacitor current feedback active damping," *Proceedings of the CSEE*, vol. 32, no. 25, pp. 133–142+19, 2012.

[8] J. Rocabert, A. Luna, F. Blaabjerg, and P. Rodríguez, "Control of power converters in AC microgrids," *IEEE Transactions on Power Electronics*, vol. 27, no. 11, pp. 4734–4749, 2012.

[9] Z. Liu, C. Zhu, Y. Wang, J. Liu, and P.. Jie, "Two improved repetitive control methods against frequency fluctuation in IPS," *Power System Technology*, vol. 042, no. 9, pp. 3014–3023, 2018.

[10] L. Zheng, F. Jiang, J. Song, Y. Gao, and M. Tian, "A discrete-time repetitive sliding mode control for voltage source inverters," *IEEE Journal of Emerging and Selected Topics in Power Electronics*, vol. 6, no. 3, pp. 1553–1566, 2018.

[11] A. Trivedi and M. Singh, "Repetitive controller for VSIs in droop-based AC-microgrid," *IEEE Transactions on Power Electronics*, vol. 32, no. 8, pp. 6595–6604, 2017.

[12] T. Hornik and Q.-C. Zhong, "A current-control strategy for voltage-source inverters in microgrids based on H-infinity and repetitive control," *IEEE Transactions on Power Electronics*, vol. 26, no. 3, pp. 943–952, 2011.

[13] T. Hornik and Q.-C. Zhong, "Hco repetitive voltage control of grid-connected inverters with a frequency adaptive mechanism," *IET Power Electronics*, vol. 3, no. 6, pp. 925–935, 2010.

[14] R. Fei, X. C. Gong, H. S. Dao, and L. Derong, "The deadbeat control strategy of modular multilevel converter," *Proceedings of the CSEE*, vol. 37, no. 06, pp. 1753–1746, 2017.

[15] M. Odavic, V. Biagini, P. Zanchetta, M. Sumner, and M. Degano, "One-sample-period-ahead predictive current control for high-performance active shunt power filters," *IET Power Electronics*, vol. 4, no. 4, pp. 414–423, 2011.

[16] J. V. Flores, L. F. A. Pereira, G. Bonan, D. F. Coutinho, and J. M. Gomes Da Silva, "A systematic approach for robust repetitive controller design," *Control Engineering Practice*, vol. 54, no. SEP, pp. 214–222, 2016.

[17] A. Lidozzi, C. Ji, L. Solero, P. Zanchetta, and F. Crescimbini, "Digital deadbeat and repetitive combined control for a stand-alone four-leg VSI," *IEEE Transactions on Industry Applications*, vol. 53, no. 6, pp. 5624–5633, 2017.

[18] A. Trivedi and M. Singh, "Repetitive controller for VSIs in droop based AC-microgrid," *IEEE Transactions on Power Electronics*, vol. 32, no. 8, pp. 6595–6604, 2016.